A Journal of the Gesellschaft Deutscher Chemiker

Angewandte International Edition GDCh Chemie

www.angewandte.org

Accepted Article

Title: Implementation of Quantum Level Addressability and Geometric Phase Manipulation in Aligned Endohedral Fullerene Qudits

Authors: Shang-Da Jiang, Shen Zhou, Jiayue Yuan, Zi-Yu Wang, Kun Ling, Peng-Xiang Fu, Yu-Hui Fang, Ye-Xin Wang, Zheng Liu, Kyriakos Porfyrakis, G. Andrew D. Briggs, and Song Gao

To be cited as: *Angew. Chem. Int. Ed.* **2021**, e202115263

Link to VoR: https://doi.org/10.1002/anie.202115263

WILEY-VCH

10.1002/anie.202115263

WILEY-VCH

RESEARCH ARTICLE

Implementation of Quantum Level Addressability and Geometric Phase Manipulation in Aligned Endohedral Fullerene Qu*d*its

Shen Zhou,*[a,b]+ Jiayue Yuan,[b,c]+ Zi-Yu Wang,[c] Kun Ling,[a] Peng-Xiang Fu,[c] Yu-Hui Fang,[c] Ye-Xin Wang,[a] Zheng Liu,[a] Kyriakos Porfyrakis,*[d,e], G. Andrew D. Briggs,[e] Song Gao,[a,c] Shang-Da Jiang*[a]

[a] Dr. S. Zhou, K. Ling, Dr. Y. Wang, Dr. Z. Liu, Prof. S. Gao, Prof. S.-D. Jiang
Spin-X Institute, School of Chemistry and Chemical Engineering, State Key Laboratory of Luminescent Materials and Devices, Guangdong-Hong Kong-Macao Joint Laboratory of Optoelectronic and Magnetic Functional Materials,
South China University of Technology
Guangzhou, China
E-mail: zhoushen@nudt.edu.cn
jiangsd@scut.edu.cn

[b] Dr. S. Zhou, J. Yuan,
College of Aerospace Science and Engineering
National University of Defense Technology
Changsha, China.

[c] Z. Wang, X. Fu, Y. Fang, Prof. S. Gao
Beijing National Laboratory of Molecular Science, Beijing Key Laboratory of Magnetoelectric Materials and Devices, College of Chemistry and Molecular Engineering
Peking University
Beijing, China

[d] Prof. K. Porfyrakis
School of Engineering
University of Greenwich
Central Avenue, Chatham Maritime, Kent, ME4 4TB, UK
E-mail: k.porfyrakis@greenwich.ac.uk

[e] Prof. G. A. D. Briggs, Prof. K. Porfyrakis
Materials Department
Oxford University
Oxford, UK

[+] These authors contributed equally to this work.

Supporting information for this article is given via a link at the end of the document.

Abstract: Endohedral nitrogen fullerenes have been proposed as building blocks for quantum information processing due to their long spin coherence time. However, addressability of the individual electron spin levels in such a multiplet system of $^4S_{3/2}$ has never been achieved because of the molecular isotropy and transition degeneracy among the Zeeman levels. Herein, by molecular engineering, we lifted the degeneracy by zero-field splitting effects and made the multiple transitions addressable by a liquid-crystal-assisted method. The endohedral nitrogen fullerene derivatives with rigid addends of spiro structure and large aspect ratios of regioselective bis-addition improve the ordering of the spin ensemble. These samples empower endohedral-fullerene-based qu*d*its, in which the transitions between the 4 electron spin levels were respectively addressed and coherently manipulated. The quantum geometric phase manipulation, which has long been proposed for the advantages in error tolerance and gating speed, was implemented in a pure electron spin system using molecules for the first time.

Introduction

Endohedral fullerenes are molecular compounds that encapsulate atoms and clusters inside the carbon cage.[1] Evidenced by the electron spin properties of N@$C_{60,70}$,[2] Sc@C_{82}, Y@C_{82}, La@C_{82},[3-4] etc., the structure essentially extends the coherence time, as it diminishes the relaxation processes related to fluctuations of environment. Moreover, the carbonaceous elemental composition can effectively sustain the spin coherence due to the zero nuclear spin of the ^{12}C. As a result, some electron-spin-based quantum applications, including molecular quantum computing,[5-6] molecular atomic clocks,[7] and quantum metrology and sensing,[8-9] have been proposed.

Chemical modifications of the fullerenes are generally beneficial to enhance their functionalities.[10] For quantum computation fine engineering at both molecular and ensemble scales is desirable to meet the scalability and addressability requirements proposed by DiVincenzo.[11] At the molecular scale, it is necessary to extend the number of non-degenerate spin transitions. This can be achieved by either covalently coupling multiple spin centers[12] or by arranging non-equidistant energy levels in high spin molecular magnets.[13] At the ensemble scale, controlling the orientations of the molecules is needed to facilitate the quantum level addressability. This is because the spin dipolar coupling and zero-field splitting (ZFS) effects have angular dependency upon the applied magnetic field.[14]

Unfortunately, endohedral fullerene chemistry is not mature enough to achieve those tasks simultaneously. Several functionalization methods for endohedral fullerenes have been reported, e.g. Prato and Bingel reactions.[15-16] There have been also multiple attempts to order fullerene ensembles using co-crystallization,[17] nanotube encapsulation,[18] substrate templating,[19] MOFs embedding,[20-21], and liquid crystal dissolving.[22-26] Considering the compatibility with the modification at the molecular scale, which may scale up to very large

10.1002/anie.202115263

structures, the liquid-crystal-assisted ordering looks attractive, since the mild solvation processing condition is more attuned to the complex molecular structures. However, the relatively weak ordering results reported to date, have been detrimental for this method, as the best ordering parameter was only 0.24,[22-23] much less than that of the liquid crystal itself.[27]

As the result of the unfulfilled molecular engineering, the coherent manipulation beyond a two-dimensional Hilbert subspace in endohedral fullerenes remains elusive. Quantum gate demonstrations that require more than two addressable energy levels such as a geometric phase gate have not been implemented with endohedral fullerenes, or even with any pure electron paramagnetic resonance (EPR) systems. In principle, the geometric phase would apply well with magnetic resonance phenomena according to initial NMR studies.[28] In NV^- centers in diamond, a crystal defect spin system possessing multi-level addressability, ODMR experiments have demonstrated the robustness of geometric phase against noise of experimental control parameters.[29] With the help of nuclear spin levels, the ENDOR implementation had also experienced a steady development from basic spinor phenomenon demonstrations[30] to useful nuclear spin applications including the bang-bang control[31] and ultra-fast entanglement.[32]

Herein, starting with rationally designed fullerene derivatives and improved liquid crystal ordering, we managed to obtain samples that simultaneously tackle the tasks of the molecular quantum systems at both molecular and ensemble scales. The chemical modification scales the spin system up to a 4-dimensional qu*d*it. The high ordering parameter O_{zz} up to 0.50 and 0.61 significantly overperforms the best results reported for fullerene alignment. Then, we manifested the multi-level addressability of the qu*d*it, using Rabi oscillation and its multi-level analogue. Finally, the first EPR demonstration of quantum geometric phase was implemented with the reported molecular system, showing that arbitrary phase shift can be readily applied by manipulations involving the auxiliary quantum level.

Results and Discussion

Chemical modification at the molecular scale

To introduce ZFS effects and lift the transition degeneracy among the Zeeman levels of endohedral nitrogen fullerenes, symmetry modification at the molecular scale is needed. Four $N@C_{60,70}$ derivatives (Scheme 1) were designed and synthesized, including two mono-functionalized derivatives (**1, 2**), a fullerene dimer (**3**), and a bis-functionalized derivative (**4**). Compared with **1** and **2**, **3** and **4** are provided with larger molecular aspect ratios due to the dimerization and bis-addition, respectively. Meanwhile, **1** and **3** have a rather flexible molecular structure, while **2** and **4** were functionalized with rigid addends with spiro structures.

All derivatives were synthesized starting from $N@C_{60}$ or $N@C_{70}$ (c.a. 0.1% spin concentration).[15] The monoadducts **1** and **2** were synthesized adopting the method of spin compatible Bingel reaction that we reported previously,[16] and characterized by UV/Vis, MALDI-TOF-MS, and ^{1}H-NMR (Figure S1).

The fullerene dimer **3** was synthesized in two steps with yields of 40% and 50%, respectively. Prato reaction was used in the first step to introduce a secondary amine group to $N@C_{60}$. Two- and ten-fold excess of amino acid and aldehyde were added to accelerate the fullerene conversion and mitigate the spin loss caused by heating.[33] Dimerization was then conducted by reacting with a stoichiometric amount of terephthaloyl dichloride. No spin loss for the endohedral fullerene was noticed during the 12-hour reaction of amidation. The HPLC, UV/Vis, MALDI-TOF-MS, and ^{1}H-NMR characterizations of **3** are shown in Figure S2.

Aiming at a bis-functionalized derivative **4**, regioselectivity is crucial. While a C_{60} cage can provide up to 8 different cis-trans isomers,[34] the reactivity difference of the reaction sites on a C_{70} cage leads to only three region-isomeric products.[35] Thereby, $N@C_{70}$ was chosen as the starting material to react with two-fold of brominated 1,3-indanedione and DBU. After a 2-hour reaction, the yield of all bis-functionalization was 85%. According to the EPR test on the aliquots throughout the reaction, the spin signal preservation ratio over 90% confirmed that the spin-compatible method we reported for mono-functionalization[16] also worked for multi-functionalization. The 2-o'clock regioisomer **4** was readily separated by preparative thin film chromatography, and further characterized by MALDI-TOF-MS, UV/Vis, ^{1}H-NMR, and ^{13}C-NMR (Figure S3).

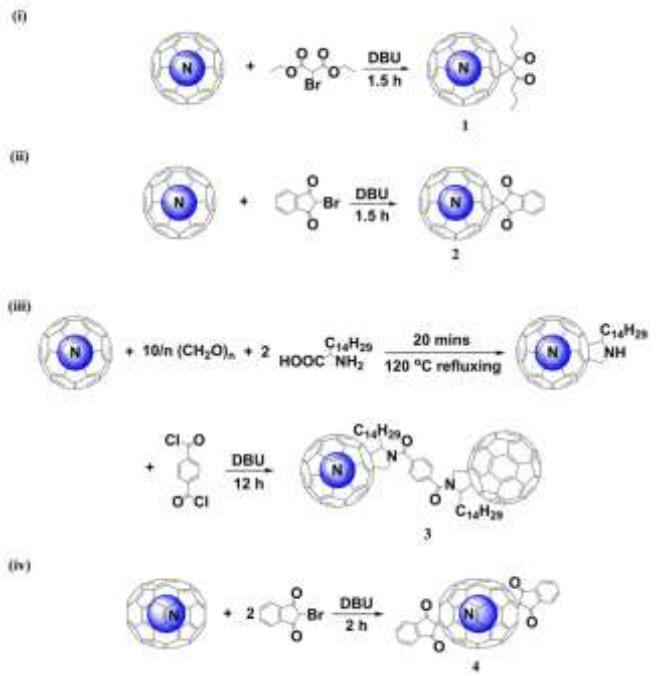

Scheme 1. Synthesis of endohedral nitrogen fullerene derivatives: mono-adducts **1** and **2**, dimer **3**, and bis-adduct **4** (2-o'clock regioisomer).

The spin Hamiltonian of the as-prepared endohedral nitrogen fullerene derivatives can be expressed as follows:

$$\hat{H} = \mu_B \vec{B}^T \bar{\bar{g}} \hat{S} + \hat{S}^T \bar{\bar{D}} \hat{S} + \hat{I}_N^T \bar{\bar{A}} \hat{S} \qquad \textbf{Eq. (1)}$$

where μ_B is the Bohr magneton, $\vec{B}$ is the external magnetic field, $\hat{S}$ is the electron spin operator, $\bar{\bar{g}}$ is the Landé matrix, $\bar{\bar{D}}$ is the ZFS tensor, $\bar{\bar{A}}$ is the hyperfine coupling tensor, $\hat{I}_N$ is the nuclear spin operator of the endohedral ^{14}N nuclei.

Figure 1a visualizes the energy levels defined by the spin Hamiltonian in Eq (1) in the high-field limit. The relatively small ZFS effect can be treated as the first order perturbation to the isotropic Zeeman splittings of S=3/2 system with small energy of ΔE_{ZFS}. The energy gaps of $|\pm 3/2\rangle \leftrightarrow |\pm 1/2\rangle$ are affected by ZFS with opposite signs, while the transition of $|-1/2\rangle \leftrightarrow |+1/2\rangle$ stays the same.

10.1002/anie.202115263

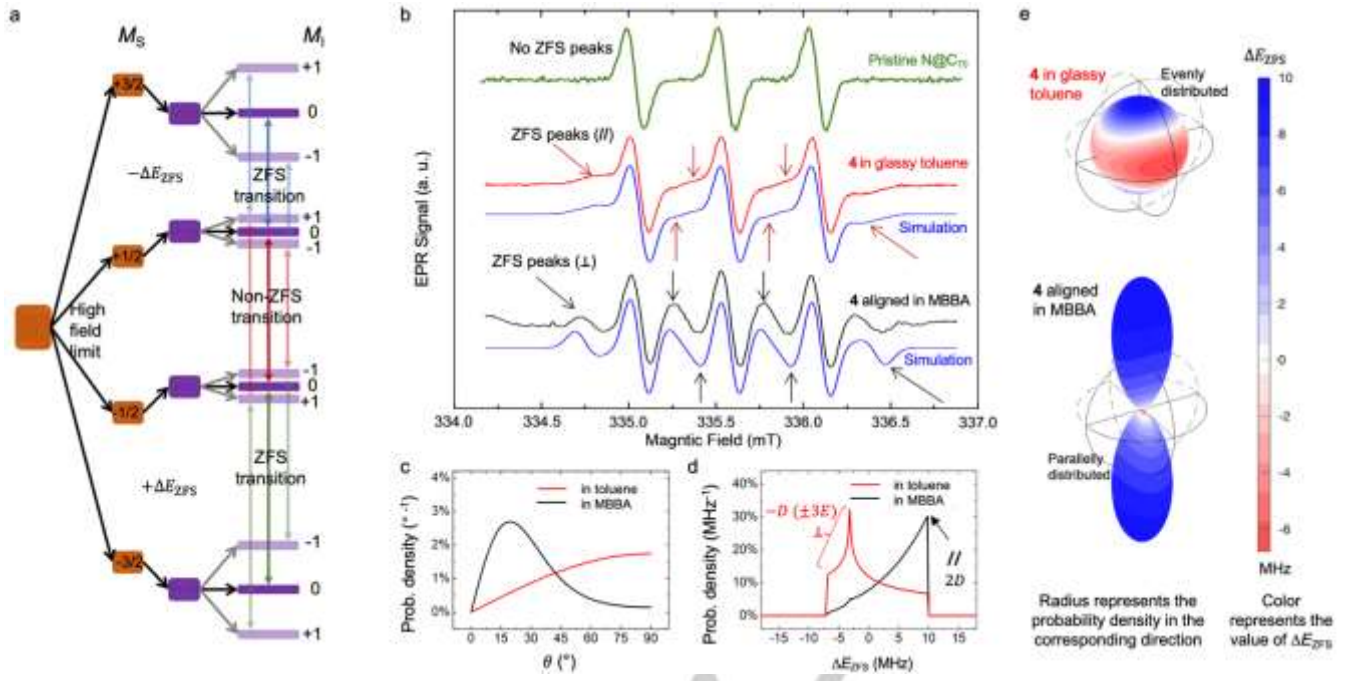

Figure 1 (a) Energy levels of endohedral nitrogen fullerene derivatives, in which the three-fold transition degeneracy of the *S* = 3/2 system is lifted by ΔE_{ZFS} due to the molecular modification. (b) CW-EPR spectra of pristine N@C_{70} and **4** in different conditions (measured at 9.41 GHz, 100 K). In contrast to the pristine sample, **4** shows characteristic side peaks caused by ZFS effect. The ZFS peak patterns of **4** in glassy toluene and **4** in aligned MBBA were also distinct. Both spectra were fitted with simulations using different molecular orientation distributions. (c) The distribution of molecular orientations of **4** in toluene and in MBBA. (d) The extracted distribution of ΔE_{ZFS} of **4** in toluene and in MBBA. (e) 3D surface color mapping of ΔE_{ZFS} for **4** in toluene and in MBBA, where the color represents the value of ΔE_{ZFS}, and the radius represents the probability.

CW-EPR spectra of all products in frozen toluene solution were applied to confirm the energy level diagram and quantify the parameters of the spin Hamiltonian. Compared to the pristine sample (Figure S4 for N@C_{60} and Figure 1b top for N@C_{70}), the Zeeman and hyperfine coupling effects were found unchanged and remain isotropic in the derivatives (Figure S4 for **1**, **2**, **3** and Figure 1b middle for **4**). The only variation of the derivatives lies in small ZFS effects $\overline{\overline{D}}$ and lead to side peaks in the spectrum.

The $\overline{\overline{D}}$ tensor is normally parameterized as the axial term D and the transverse term E in its principal axis. According to EasySpin[36] fitting of the CW-EPR spectra of the frozen solutions, the ZFS parameters of the four endohedral nitrogen derivatives are **1** ($|D| = 8.4$ MHz, $E = 0.4$ MHz), **2** ($|D| = 8.9$ MHz, $E = 0.6$ MHz), **3** ($|D| = 14.7$ MHz, $E = 0.6$ MHz), and **4** ($|D| = 5.0$ MHz, $E = 0.7$ MHz), respectively. The emergence of ZFS effects can be further verified by DFT calculations on the spin distribution of the products (Figure S5). The chemical modification on the molecular scale can slightly affect the anisotropy of the spin center, and the principal axis of $\overline{\overline{D}}$ tensor is along the addend direction.

With the ZFS parameters and principal axis been determined, one can unravel the perturbation energy of the angular-dependent ΔE_{ZFS}. When the long axis of the molecule parallels the magnetic field (experimental frame), ΔE_{ZFS} equals to $2|D|$. In general, Euler rotation matrix of $\overline{\overline{R}}(\theta, \varphi, 0)$ is needed to transform the ZFS tensor frame to the experimental one, the value of ΔE_{ZFS} is calculated to be $(3\cos^2\varphi - 1)D - 3\sin^2\varphi\,(2\sin^2\theta - 1)\,E$.

Axial alignment at the ensemble scale

After the transition degeneracy is successfully lifted by ΔE_{ZFS} at the molecular scale, we then respectively dissolve the four derivatives in a liquid crystal MBBA (N-(4-Methoxybenzylidene)-4-butylaniline) to refine the magnetic anisotropy of the endohedral fullerene systems in the ensemble level. At first, the MBBA solution samples were aligned in the magnetic field (350 mT) at room temperature in the nematic phase, and then *in-situ* frozen to 100 K rapidly to lock the orientation. The host molecules of MBBA were aligned parallel to the external magnetic field, due to the diamagnetism of the liquid crystal domains.[27] The host matrix further induces the guest fullerenes to orient along the field by the Van der Waals interaction.[22] Conversely, the magnetic dipolar field of the paramagnetic spin (< 2 mT in a 1 nm distance) was estimated to be too weak to align directly by the external field nor alter the behavior of liquid crystals.

The orientation distribution of the guest molecules can be deduced by studying the spin anisotropy. Taking **4** as an example, Figure 1b compares its CW-EPR spectra in frozen toluene and in MBBA at 100 K. The angular-dependent peaks corresponding to $|\pm 3/2\rangle \leftrightarrow |\pm 1/2\rangle$ transitions showed differently. Both spectral patterns can be simulated and fitted by different molecular orientations obeying Boltzmann distribution. The distribution density $p(\beta)$ is defined by the axially ordering potential applied by the environment:

$$p(\beta) = \exp\left(\frac{-U(\beta)}{k_{\mathrm{B}}T}\right) / \int \exp\left(\frac{-U(\beta)}{k_{\mathrm{B}}T}\right)\sin\beta \mathrm{d}\beta \qquad \textbf{Eq. (2)}$$

$$U(\beta) = k_{\mathbf{B}}TC_{20}D^2_{0,0}(\beta) \qquad \textbf{Eq. (3)}$$

where β is the molecular long axis with respect to the host, T is the temperature, k_{B} is the Boltzmann constant, $U(\beta)$ is the axial ordering potential, C_{20} is the axial ordering potential coefficient, and $D^2_{0,0}(\beta)$ is the element of Wigner *D*-matrix.[37]

10.1002/anie.202115263

In the powder-like spectrum of **4** dispersed in glassy toluene (Figure 1b middle), the best fit using the Boltzmann distribution shows that the C_{20} equals 0, meaning no preferential orientation (Figure 1c). The value of the ZFS perturbation energy ΔE_{ZFS} was illustrated with a 3D surface color mapping showing the angular dependency (Figure 1e), and the distribution of ΔE_{ZFS} can be worked out by integrating over all orientations (Figure 1d). In the aligned sample (Figure 1b bottom), the least square fitting of spectrum suggests that its C_{20} equals to $3.0\ (\pm 0.1)$. The large axial ordering potential coefficient shifts the preferred orientation of the molecule to the parallel direction of the magnetic field (Figure 1c), so the 3D surface is reshaped with enlarged radii in the parallel directions, and diminished radii in the perpendicular directions, with the radius representing the probability density (Figure 1e). The distribution of ΔE_{ZFS} (Figure 1d) preferring the parallel orientation is also obtained. Such behavior is consistent with the spectrum, proving that the large axial ordering potential coefficient is reasonable.

Ordering parameter $O_{zz} = (3\langle\cos^2\beta\rangle - 1)/2$ is applied to quantitatively describe the distribution of axially ordered **4**. An O_{zz} of $0.61\ (\pm 0.02)$ can be derived. The ordering parameters were also determined from the CW-EPR spectra (Figure S6) for the other derivatives (**1**: $O_{zz} = 0.29(\pm 0.02)$, **2**: $O_{zz} = 0.50(\pm 0.02)$, **3**: $O_{zz} = 0.10(\pm 0.02)$). Table 1 compares the order parameters reported for liquid-crystal-assisted alignment of endohedral fullerenes and other relevant systems. Both **2** and **4** with the spiro structure show high ordering parameters, suggesting that rigidity is the primary factor for good alignment. The discovery is consistent with the trend of nitroxide C_{60} derivatives reported previously.[22,25] **4** having the highest ordering parameter shows that a large aspect ratio is also beneficial, but rigidity must be achieved as a precondition, since the longer dimer of **3** has no improvement at all compared to **1**. It is also worth noting that **1**, which has the same addend as a previously reported photoexcited cyclopropane C_{60},[24] did not reproduce an ordering parameter as high. This could probably be attributed to the orientational preference of spin stimulation and relaxation during the photoexcitation and phosphorescence procedures. The lower ordering parameter reported in this work should be more representative for the actual morphological orientation distribution of the whole molecular system.

Table 1. Comparison of order parameters of different fullerene (derivatives) in liquid crystals.[23-27]

Endohedral Fullerene (derivatives)	O_{zz}	Relevant system	O_{zz}
3	0.10	Nitroxide C_{60} derivative with flexible addend[22]	0.11
N@C_{70}[23]	0.18	Nitroxide C_{60} derivative with rigid addend[25]	0.48
N@C_{60} pyrrolidine derivatives[23]	0.24	Photoexcited Bis-cyclopropane C_{60}[24]	0.29-0.52[a]
1	0.29	Photoexcited Mono-cyclopropane C_{60}[24]	0.52[a]
2	0.50		
4	0.61	MBBA liquid crystal[27]	0.62

[a] Transient spin systems may be selectively stimulated.

As far as we are aware, this is the highest degree of alignment ever reported, for any endohedral fullerene system within liquid crystals. The high ordering parameters for **2** and **4** (with rigid addends) are almost as high as the host molecule of MBBA itself ($O_{zz} = 0.62$).[27] A series of angular-resolved CW-EPR results on **2** and **4** (Figure S7 and S8) were acquired to further prove good alignment is achieved. At the perpendicular direction ($\lambda = 90^o$), the narrowest molecular orientation distribution was achieved, so that the best addressability of individual transitions can be enabled in these conditions.

Coherent addressability of the quantum levels

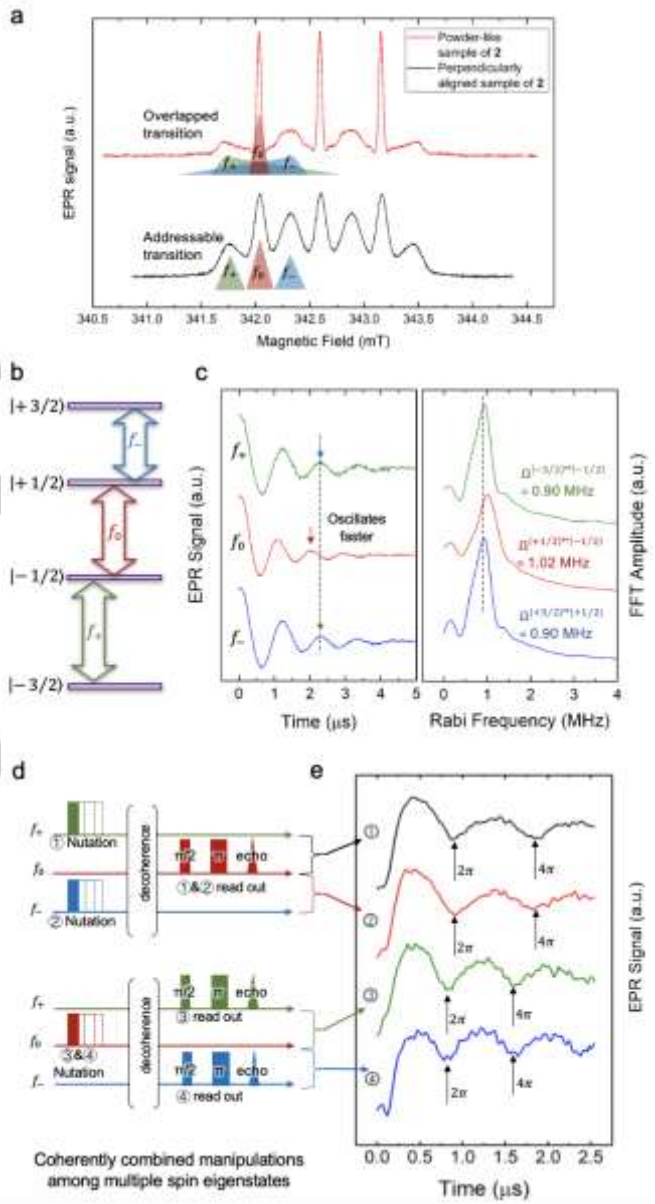

Figure 2 (a) EDFS showing that the aligned sample can separately address the three transitions, while the powder-like sample has overlapping issues. (b) Four energy levels of the electron spin and the corresponding transition frequencies. (c) Standard nutation experiments of each transition with the Rabi frequency determined by fast Fourier transformations. (d) Pulse sequences of multilevel Rabi oscillations using nutation and read out pulses pumped with different transitions. (e) Spectra of multilevel nutation experiments showing the coherence between all four energy levels. (All experiments were conducted at 80 K, using **2** perpendicularly aligned to the magnetic field)

10.1002/anie.202115263

Using the perpendicular alignment, we took **2** dissolved in MBBA as an example to demonstrate the quantum level addressability using pulsed EPR experiments. The echo-detected-field-sweep (EDFS) spectra (Figure 2a) showed better separated transition peaks in the aligned sample, in contrast to the powder-like one. The transition peaks labeled f_+, f_0, and f_- are the frequency channels to pump the microwave pulses and manipulate the S = 3/2 spin.

As Figure 1a illustrates, the full spin system contains 12 eigenstates, but the nuclear spin will not be altered during a pulsed-EPR experiment. Thus, only four energy states highlighted in Figure 2b are relevant in the pulsed EPR experiments. Performing standard Rabi oscillation experiments with these transitions, $|+1/2\rangle \leftrightarrow |-1/2\rangle$ oscillates 13% faster than $|\pm 3/2\rangle \leftrightarrow |\pm 1/2\rangle$ (Figure 2b), which is consistent with the desired Rabi frequency ratio of $\sqrt{3} : 2$ calculated by the following equations:

$$\Omega^{M_S \leftrightarrow M_{S+1}} = \mu_B g B_1 \sqrt{S(S+1) - M_S(M_S+1)} \qquad \textbf{Eq. (4)}$$

where Ω is the Rabi frequency, μ_B is the Bohr magneton, g is the Landé factor, B_1 is the magnetic field amplitude of the microwave pulse, S is the spin quantum number, and M_S is the spin magnetic quantum number.

Multilevel nutation experiments were also successfully conducted to prove that the four energy levels are coherently controllable. As Figure 2d depicts, nutations between $|\pm 3/2\rangle \leftrightarrow |\pm 1/2\rangle$ can manipulate the population difference between $|+1/2\rangle$ and $|-1/2\rangle$, and vice versa. In contrast to the conventional Rabi oscillation, the EPR signal increases in the beginning, because the population differences are enlarged by the nutation pulses when the initial condition of the spin system follows a thermal equilibrium distribution at 80 K. The Rabi frequencies in Figure 2d were only affected by the energy levels where the nutation pulses were applied on, but do not depend on the detection sequence. Consistent with Figure 2c, the nutation in $|+1/2\rangle \leftrightarrow |-1/2\rangle$ transition is faster.

Spinor behavior and geometric phase manipulation

The quantum geometric phase (or Berry phase) is one of the most intriguing aspects of the nature of quantum systems. A coherent EPR demonstration of it has been proposed for more than 30 years,[38] but has never been achieved. This is mainly because the majority of EPR systems are isolated single qubit systems that lack an addressable auxiliary energy level within the bandwidth of coherent manipulation to demonstrate the geometric phase. Utilizing the addressable spin system of endohedral fullerene qu*d*it, we sequentially conducted the spinor behavior experiment (a special case of geometric phase) and general geometric phase experiments. The pulse sequences are illustrated in Figure 3a and b, respectively.

Both experiments start with initialization operations to populate the eigenstate of $|-3/2\rangle$ forming a pseudo pure state. Then, superpositions between $|-3/2\rangle$ and $|-1/2\rangle$ were prepared with a Hadamard pulse. Without additional manipulations, it gives a standard Hahn echo by a π pulse with an interval of τ. The quantum phases of the superposition states remain constant in the rotational framework defined by the detection frequency of f_+. Additional pulses were applied via the transition involving the auxiliary energy level $|+1/2\rangle$, during the waiting time τ (Figure 3a and b), and the influence on the quantum phase was tested.

For the spinor behavior test, the additional pulse is applied with varied durations. As the results show (Figure 3c), the phase of the Hahn echo shifts with the increased length. When the tipping angle equals to 2π, which is a full period that nutates the spin with the $|+1/2\rangle \leftrightarrow |-1/2\rangle$ transition, the Hahn echo phase of the $|-3/2\rangle$ and $|-1/2\rangle$ superposition experiences a 180-degree flip. This demonstrates the spinor nature of the electron spin: similar to a vector pointing along the Möbius band, it exhibits a sign inversion when the system is rotated through a full turn. The decreasing trend of the echo intensity is attributed to the shorter relaxation time of the superposition state of $|-3/2\rangle$ and $|+1/2\rangle$ (double-quantum coherence state) than that of $|-3/2\rangle$ and $|-1/2\rangle$.

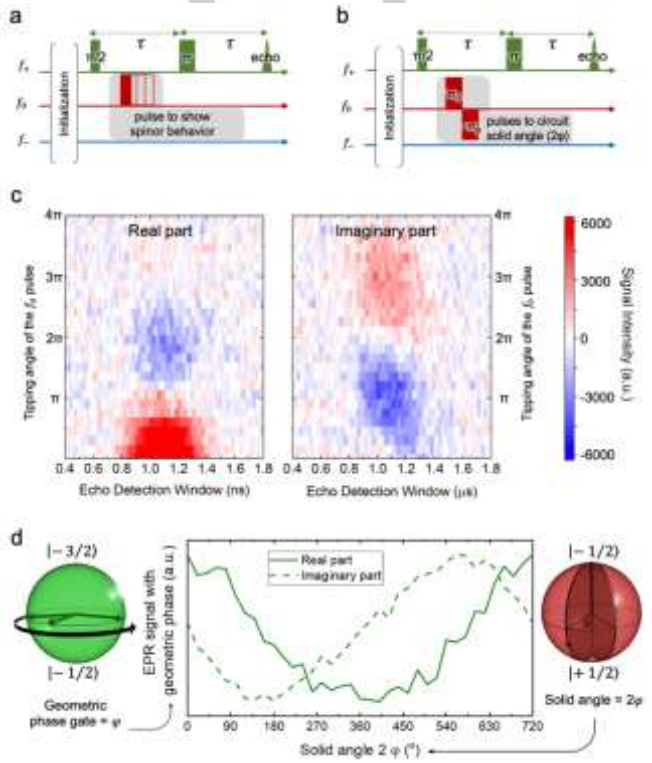

Figure 3 (a) Pulse sequences of the spinor experiment. (b) Pulse sequences of the geometric phase experiment (c) Echo evolution in the ($|-3/2\rangle \leftrightarrow |-1/2\rangle$) transition with the increased spinor pulse duration in the $|+1/2\rangle \leftrightarrow |-1/2\rangle$ transition. (d) Arbitrary geometric phase imposed on the superposition state of $|-3/2\rangle$ and $|-1/2\rangle$, by controlling the solid angle that the $|+1/2\rangle \leftrightarrow |-1/2\rangle$ transitions experience. (Both experiments were conducted at 80 K, using **2** perpendicularly aligned to the magnetic field)

For the general geometric phase experiment, the auxiliary pulses are a π and a -π_φ pulse, where φ is the phase of the pulse controlled by arbitrary wave generator (AWG). The combination of the two pulses forms a solid angle of 2φ in the Bloch sphere of $|+1/2\rangle$ and $|-1/2\rangle$. The geometric phase equals half of the solid angle, which should be φ. Indeed, the evolution of the integrated intensity of the spin echo acquired by a quadrature detector (Figure 3d) manifests that an arbitrary phase gate of φ in the superposition state of $|-3/2\rangle$ and $|-1/2\rangle$ (shown by the Bloch sphere in green) can be readily applied by pulses in the auxiliary transition that circuit a solid angle of 2φ (shown by the Bloch sphere in red). When the solid angle $2\varphi = 2\pi$, the geometric phase experiment is equivalent to the spinor behavior experiment.

Compared with other coherent manipulation methods such as spin nutation, the geometric phase manipulation only depends on the solid angle of the path and is resilient to errors of the pulse duration and intensity. An evaluation of the error tolerances effect of the geometric phase gate is beyond the scope of this paper emphasizing enabling addressability with chemistry, but a quantitative fidelity comparison will be discussed in a separate work.

To summarize, the pulsed-EPR experiments proved that coherent manipulations can be accomplished by selectively addressing the transitions. To the best of our knowledge, this is the first geometric phase demonstration using EPR. It is also worth noting that, benefiting from the long relaxation time of endohedral nitrogen fullerene, these results were all acquired above the liquid nitrogen temperature and did not use deuterated solvents to further improve the spin environment. We believe that more sophisticated manipulations such as Grover algorithm can be demonstrated in this system with optimizations in the near future.

Conclusion

Four types of chemical functionalizations of endohedral nitrogen fullerene were conducted, lifting the degeneracy of the transitions in the S = 3/2 spin system. Fullerene derivatives with spiro-addends and good rigidity align properly in liquid crystal, and large aspect ratio achieved by regioselectivity further increase the ordering parameter up to $O_{zz} = 0.61$. With the aligned sample, quantum level addressability was experimentally demonstrated by coherent manipulations. Moreover, the spin system enabled us to perform the first geometric phase manipulations in molecular-based electron spin systems. The reported alignment approach could be further adapted to other endohedral fullerene systems of high spin or even multi-spin systems to expand the scalability of the quantum systems. It also shed light on new solutions to fullerene spin optical pumping and fullerene spin gyroscope where molecular orientational ordering is required.

Acknowledgements

This research is supported by National Key R&D Program of China (2017YFA0204903 and 2018YFA0306003), National Natural Science Foundation of China (U20A6002, 21822301, 51802346), Beijing Academy of Quantum Information Sciences (Y18G23), and Open Funds of the State Key Laboratory of Rare Earth Resource Utilization (RERU2020003). KP thanks EPSRC for support (EP/K030108/1).

Keywords:· fullerenes ·geometric phase · liquid crystals ·molecular qu*d*its· spiro compounds

[1] A. A. Popov, S. Yang, L. Dunsch, Chem. Rev. **2013**, *113*, 5989–6113.
[2] J. J. L. Morton, A. M. Tyryshkin, A. Ardavan, K. Porfyrakis, S. A. Lyon, G. Andrew D. Briggs, J. Chem. Phys. **2006**, *124*, 14508.
[3] K. Kikuchi, Y. Nakao, S. Suzuki, Y. Achiba, J. Am. Chem. Soc. **1994**, *116*, 9367–9368.
[4] R. M. Brown, Y. Ito, J. H. Warner, A. Ardavan, H. Shinohara, G. A. D. Briggs, J. J. L. Morton, Phys. Rev. B **2010**, *82*, 033410.
[5] J. Morton, A. M. Tyryshkin, A. Ardavan, S. C. Benjamin, A. Briggs, Nat. Phys. **2006**, *2*, 40–43.
[6] Y. X. Wang, Z. Liu, Y. H. Fang, S. Zhou, S. Da Jiang, S. Gao, npj Quantum Inf. **2021**, *7*, 32.
[7] R. T. Harding, S. Zhou, J. Zhou, T. Lindvall, W. K. Myers, A. Ardavan, G. A. D. Briggs, K. Porfyrakis, E. A. Laird, Phys. Rev. Lett. **2017**, *119*, 140801.
[8]. T. Wakahara, T. Kato, K. Miyazawa, W. Harneit, Carbon **2012**, *50*, 1709–1712.
[9] S. P. Cornes, S. Zhou, K. Porfyrakis, Chem. Commun. **2017**, *53*, 12742-12745.
[10] S. S. Babu, H. Möhwald, T. Nakanishi, Chem. Soc. Rev. **2010**, *39*, 4021–4035.
[11] D. P. DiVincenzo, *Fortschritte der Phys.* **2000**, *48*, 771–783.
[12] F. Lombardi, A. Lodi, J. Ma, J. Liu, M. Slota, A. Narita, W. K. Myers, K. Müllen, X. Feng, L. Bogani, *Science* **2019**, *366*, 1107–1110.
[13] M. N. Leuenberger, D. Loss, *Nature* **2001**, *410*, 789–793.
[14] Y.-H. Fang, Z. Liu, Y.-X. Wang, S. Zhou, S.-D. Jiang, S. Gao, *Inorg. Chem. Front.* **2020**, *7*, 3875–3881.
[15] S. Zhou, M. Yamamoto, G. A. D. Briggs, H. Imahori, K. Porfyrakis, J. Am. Chem. Soc. **2016**, *138*, 1313–1319.
[16] S. Zhou, I. Rašović, G. A. D. Briggs, K. Porfyrakis, Chem. Commun. **2015**, *51*, 7096–7099.
[17] Y.-Y. Xu, H.-R. Tian, S.-H. Li, Z.-C. Chen, Y.-R. Yao, S.-S. Wang, X. Zhang, Z.-Z. Zhu, S.-L. Deng, Q. Zhang, S. Yang, S.-Y. Xie, R.-B. Huang, L.-S. Zheng, Nat. Commun. **2019**, *10*, 485.
[18] B. Smith, M. Monthioux, D. Luzzi, Nature **1998**, *396*, 323–324.
[19] D. S. Deak, K. Porfyrakis, M. R. Castell, Chem. Commun. **2007**, *43*, 2941–2943.
[20] Y. Feng, T. Wang, Y. Li, J. Li, J. Wu, B. Wu, L. Jiang, C. Wang, J. Am. Chem. Soc. **2015**, *137*, 15055–15060.
[21] J. Zhang, C. Zhao, H. Meng, M. Nie, Q. Li, J. Xiang, Z. Zhang, C. Wang, T. Wang, Carbon **2020**, *161*, 694–701.
[22] G. Liu, M. del C. Gimenez-Lopez, M. Jevric, A. N. Khlobystov, G. A. D. Briggs, K. Porfyrakis, J. Phys. Chem. B **2013**, *117*, 5925–5931.
[23] C. Meyer, W. Harneit, K. Lips, A. Weidinger, P. Jakes, K. P. Dinse, Phys. Rev. A **2002**, *65*, 061201.
[24] M. Bortolus, A. Ferrarini, J. van Tol, A. L. Maniero, J. Phys. Chem. B **2006**, *110*, 3220–3224.
[25] M. Mazzoni, L. Franco, A. Ferrarini, C. Corvaja, G. Zordan, G. Scorrano, M. Maggini, Liq. Cryst. **2002**, *29*, 203–208.
[26] H. K. Bisoyi, S. Kumar, Chem. Soc. Rev. **2011**, *40*, 306–319.
[27] R. Chang, Mol. Cryst. Liq. Cryst. **1975**, *30*, 155–165.
[28] J. A. Jones, V. Vedral, A. Ekert, G. Castagnoli, Nature **2000**, *403*, 869-871
[29] C. G. Yale, F. J. Heremans, B. B. Zhou, A. Auer, G. Burkard, D. D. Awschalom, Nat. Photo. **2016**, *10*, 184-189.
[30] D. Suter, A. Pines, M. Mehring, Phys. Rev. Lett. **1986**, *57*, 242-244
[31] J. J. L. Morton, A. M. Tyryshkin, A. Ardavan, S. C. Benjamin, K. Porfyrakis, S. A. Lyon, G. A. D. Briggs, Nat. Phys. **2006**, *2*, 40-43
[32] V. Filidou, S. Simmons, S. D. Karlen, F. Giustino, H. L. Anderson, J. J. L. Morton, Nat. Phys. **2012**, *8*, 596-600
[33] B. J. Farrington, M. Jevric, G. A. Rance, A. Ardavan, A. N. Khlobystov, G. A. D. Briggs, K. Porfyrakis, Angew. Chemie - Int. Ed. **2012**, *51*, 3587–3590.
[34] J. Nierengarten, V. Gramlich, Angew. Chemie **1996**, *108*, 2242–2244.
[35] C. Thilgen, A. Herrmann, F. Diederich, Angew. Chemie Int. Ed. **1997**, *36*, 2268–2280.
[36] S. Stoll, A. Schweiger, J. Magn. Reson. **2006**, *178*, 42–55.
[37] P. L. Nordio, P. Busolin, J. Chem. Phys. **1971**, *55*, 5485.
[38] D. Gamliel, J. H. Freed, Phys. Rev. A **1989,** 39, 3238-3255.

10.1002/anie.202115263

WILEY-VCH

RESEARCH ARTICLE

Entry for the Table of Contents

Insert graphic for Table of Contents here. ((Please ensure your graphic is in **one** of following formats))

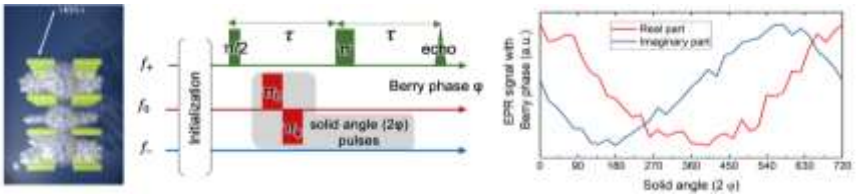

Insert text for Table of Contents here. ((The Table of Contents text should give readers a short preview of the main theme of the research and results included in the paper to attract their attention into reading the paper in full. The Table of Contents text **should be different from the abstract** and should be no more than 50-60 words long.))

Toward molecular quantum computing, the system needs to have good coherence, scalability, and addressability. Using endohedral nitrogen fullerenes with long coherence time, this work tackled the remaining two challenges by molecular modification and ensemble alignment. The refined molecular system scales up to four addressable quantum levels and enables the first implementation of geometric phase manipulation using pure electron paramagnetic resonance.

Institute and/or researcher Twitter usernames: ((optional))

NA